Gold Nanorods with Sub-Nanometer Separation using Cucurbit[*n*]uril for SERS Applications

*Samuel T. Jones, Richard W. Taylor, Rubén Esteban, Enass K. Abo-Hamed, Paul H. H. Bomans, Nico A. J. M. Sommerdijk, Javier Aizpurua, Jeremy J. Baumberg, and Oren A. Scherman**

Noble metal nanoparticles have the unique ability to guide and localize light at the nanometer scale, a feature at the heart of the field of plasmonics. Upon exposure to light, nanoparticles exhibit free electron oscillations referred to as localized surface plasmon resonances.[1–3] The resonance energy of this nanoparticle plasmon is sensitive to the particle size, shape, local environment and crucially, proximity to other plasmon-sustaining nanoparticles.[4,5] Gold nanorods (AuNRs) are anisotropic nanoparticles that exhibit well-defined optical properties and have attracted much attention in biomedical applications such as bioimaging,[6] biosensing[7–9] and photothermal therapy.[10] For each distinct axis, nanorods support a unique plasmon mode, where the energy of each resonance is dependant on the length. For prolate nanorods there are two distinct resonances, the transverse and longitudinal, corresponding to electron oscillations along the short and long axes of the nanorod. For nanorods aligned end-to-end, and spaced less than their width apart, the individual longitudinal dipole plasmons couple strongly together, resulting in a lowering of the resonance energy.[11,12] The red-shift in the peak energy of coupled plasmon absorption is determined crucially by the inter-particle distance (l_{gap}).[13] Aggregation of additional rods into the chain further shifts the mutual coupled resonance (creating a chain plasmon). Additionally, the nano-junction between the rods leads to the accumulation of a very large electric field enhancement in the interstitial gap.

This localized enhancement in the nano-junction may be exploited for applications such as surface-enhanced Raman spectroscopy (SERS).[14–16] Crucially, the strength of the field enhancement is highly dependent upon nanoparticle separation. The largest and thus most desirable field enhancements occur for $l_{gap} \approx 1$ nm.[14,17] However, the ability to reproducibly define and control the interstitial junctions where these intense field amplifications occur (so called "hot-spots") for sub-nanometer distances is a significant challenge.

Aligning AuNRs end-to-end using a number of approaches, including supramolecular assembly,[18,19] solvent interactions,[20–23] lithography[24] and other techniques have been presented. However the majority of published work focuses on achieving long chain lengths with little or no control, or reproducibility, of the crucial inter-rod separations. Work by Kumacheva et al. has perhaps made the most significant advances in controlling such parameters when aligning AuNRs. They have shown that the coupling between AuNRs can be used to determine the degree of AuNR assembly as well as highlighting that such assemblies are useful for SERS applications.[25,26] However such an approach to assembly is only able to obtain, at the smallest, inter-rod separations of 8.2 ± 1.1 nm. Recently, Mirkin et al. used elegant lithographic techniques to highlight the importance of AuNR separations <2 nm, noting that at these small separation distances high enhancement factors are achievable and important for SERS applications.[24] However, large scale solution-phase methods, leading to reproducible inter-rod separations that are <5 nm have yet to be achieved.

It was recently shown that cucurbit[*n*]urils (CB[*n*]s) are capable of reproducibly controlling the desired distance between spherical nanoparticles by acting as a rigid spacer, defining the separation to be 0.9 nm.[27–30] CB[*n*]s are rigid macrocycles consisting of *n* glycoluril repeat units, where *n* = 5–8. In addition to spacing the inter-particle junction, CB[*n*]s also have a hydrophobic cavity capable of guest incorporation, thus placing the SERS target molecule in the

S. T. Jones, E. K. Abo-Hamed, Dr. O. A. Scherman
Melville Laboratory for Polymer Synthesis
Department of Chemistry
University of Cambridge
Cambridge, CB2 1EW, UK
E-mail: oas23@cam.ac.uk
Dr. R. W. Taylor, Prof. J. J. Baumberg
Nanophotonics Centre
Cavendish Laboratory
University of Cambridge
Cambridge, CB3 0HE, UK
Dr. R. Esteban, Prof. J. Aizpurua
Material Physics Center CSIC-UPV/EHU and
Donostia International Physics Center DIPC
Paseo Manuel Lardizabal 5, San Sebastián 20018, Spain
Dr. R. Esteban
Quantum Measurement Division and Joint Quantum Institute
National Institute of Standards & Technology and
University of Maryland
Maryland 20899-8423, USA
Dr. P. H. H. Bomans, Prof. N. A. J. M. Sommerdijk
Laboratory of Materials and Interface Chemistry &
Soft Matter CryoTEM Research Unit
Department of Chemical Engineering and
Chemistry, and Institute for Complex Molecular Systems
Eindhoven University of Technology
PO Box 513, 5600 MB Eindhoven, The Netherlands

DOI: 10.1002/smll.201401063

NANO MICRO small

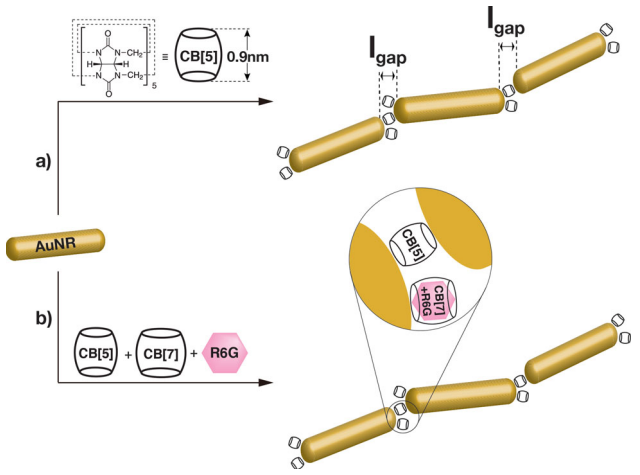

Figure 1. Scheme representing a) the alignment of AuNRs via CB[5] giving a defined separation distance of 0.9 nm (l_{gap}) and b) the alignment of AuNRs via a 1:1 mixture of CB[5] and CB[7], gives structures capable of encapsulating guests from solution.

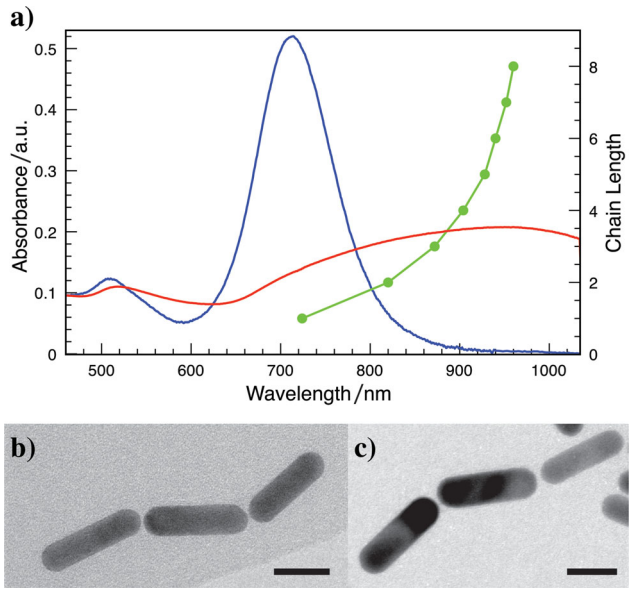

Figure 2. a) Visible to near infrared (Vis–NIR) spectra showing effect of washing untreated AuNRs (blue) against a CB[5] solution (red) twice and peak of the long wavelength resonance λ_{max} vs the number of AuNRs per chain taken from full electrodynamical calculations (green). The inter-rod separation distance is assumed to be of 1 nm in these calculations. b,c) TEM images showing alignment of AuNRs after washing with CB[5]. Scale Bars = 20 nm.

very center of the hot-spot for optimal SERS sensing.[28] CB[*n*] as a molecular SERS container is particularly desirable as it allows for the sensing of analytes at the metal surface that have no affinity for the surface, or are not soluble in water, such as coumarin.[29] However it is highly non-trivial to extend this work from spherical nanoparticles to nanorods, due to the required anisotropic binding.

Here, solution-phase synthesis in combination with the unique binding ability of CB[*n*] are used to align AuNRs and provide precise and reproducible control over the AuNR separation distance of 0.9 nm (**Figure 1**). Full electromagnetic simulations of the optical extinction matches those seen from the experimental AuNR chains. In addition, alongside the ability of CB[*n*] to incorporate guest molecules, our large enhancements achieved are exploited to detect a standard Raman dye, rhodamine 6G (R6G), in solution using SERS.

AuNRs with an aspect ratio of 3.3 (36 nm long × 11 nm thick) were synthesized by the well-documented seed-mediated technique.[21] AuNRs of this size give rise to plasmon modes at 510 nm and 712 nm for the transverse and longitudinal modes, respectively. In this aqueous phase synthetic technique, gold nanoparticle (AuNP) seeds are added to a cetyltrimethylammonium bromide (CTAB) and gold salt (Au^{3+}) growth solution. Upon addition of a mild reducing agent, the Au^{3+} salt is reduced and begins to add to the AuNP seeds. On account of the concentrated CTAB environment the growth is controlled to yield a rod like geometry.[31] This leads to AuNRs coated by a bilayer of CTAB molecules, which are more tightly bound along the {100} longitudinal facet of each rod compared with the curved {111}-end facets.[32] Removal of CTAB from the {100} facets is significantly more challenging than removal from the {111} facets. Functionalization of the {100} facet has been shown to require the use of additional solvents, such as ethanol, which destabilizes the CTAB bilayer.[33] By contrast, functionalization of the curved {111}-end facets occurs far more easily, which has allowed for the preferential end-functionalization of AuNRs.[18–20,22]

This unique property is exploited to allow alignment of AuNRs using CB[*n*] yielding defined and reproducible separation distances of <1 nm. An aqueous solution of AuNRs was centrifuged to remove excess CTAB followed by the addition of a 1:1 solution of H_2O:CB[5] (1 mM), which was repeated twice. This process preferentially destabilized the CTAB bilayer at the curved {111} end facets of the AuNRs so that upon addition of CB[5], alignment occurs in an end-to-end manner. After one centrifuge wash cycle a small blue shift was observed in the longitudinal mode, which is typically associated with the removal of excess CTAB.[34] No significant shifts were observed until another centrifuge wash cycle was conducted and the CB[5] concentration exceeded that of the initial CTAB concentration. After two wash cycles, CTAB is only weakly associated at the rod ends. Upon further addition of CB[5], the peak resonance wavelength of the longitudinal mode red-shifts dramatically to the IR region of the spectrum (**Figure 2**), placing the absorbance in the centre of the biologically relevant range for imaging. This large shift of the longitudinal mode and small shift in the transverse mode is characteristic of AuNR end-to-end alignment.[12,21,22] It was also possible to align the AuNRs by addition of double the amount of CB[5] after two successive water washes, although this method led to some undesired precipitation of AuNRs.

The extent of the red-shift indicated end-to-end assembled AuNRs with very small inter-rod separations and is consistent with results obtained from full electrodynamical calculations (Figure 2). The position of the lowest energy dipolar extinction peak, as obtained from a calculation of a straight linear chain of rods separated by a 1 nm gap is shown in Figure 2a. For longer chains, the peak is located at lower energies, with a saturation of the red-shift being observed

as more rods are added. The peak for single particles corresponds well to the measured result for unwashed rods, while the broad peak obtained experimentally with CB[5] covers the spectral range where the calculated chain resonances are found. Thus, this broad spectra is interpreted as an average of the spectra of linear chains of different lengths.

Transmission electron microscopy (TEM) was undertaken on samples after two centrifuge wash cycles with CB[5]. Conventional TEM analysis yielded only a small number of short AuNR chains and a number of larger aggregates, likely due to undesirable aggregation upon drying (Figure 2b,c). Analysis of the AuNR separation distances reveals that the average separation was 1.0 ± 0.3 nm, which is consistent with previous observations[28] and with the expected height of one CB molecule.[35] Cryo-TEM avoided drying effects and analysis of the obtained micrographs highlighted the size of the aggregates formed in solution,[36] with the observed structures being consistent with visible to near infrared (Vis–NIR) spectroscopy and predictions from our electromagnetic calculations. The use of cryo-TEM also allowed for tomographic imaging to be conducted on the aligned chains (**Figure 3**e), rendering a better understanding of the three-dimensional structure of the aligned AuNRs.

To understand the details of the spectra observed in Figure 2, we perform additional simulations of the optical response of AuNR chains in water, considering the presence of kinks along the chains as observed in the Cryo-TEM images in Figures 3. We model straight linear chains with a boundary element method (BEM[37]), and kinked disordered chains with a multiple multipole method (OpenMax).[38,39] In all simulations, the modelled rods are rotationally symmetric, 36 nm long, have a 11 nm diameter, and a plane-wave illumination with wave-vector perpendicular to the plane containing the chain is considered. A permittivity of $\varepsilon_{(H_2O)} = 1.77$ for water and the dielectric values for Au from Johnson and Christy[40] are used.

We first consider the effect of disorder in the chains. We have previously shown that the long-wavelength dipolar modes of chains formed by spherical particles are quite insensitive to disorder.[41] A similar behavior is observed here for AuNR chains when comparing a perfectly linear structure and a disordered configuration with significant kinks (**Figure 4**a). The l_{gap} between the five rods constituting each chain is 1 nm, and the indicated electric field polarization was chosen to excite the longitudinal mode along the chain. The lowest energy dipolar extinction peak is observed at a wavelength near 925 nm for the two geometries being compared (Figure 4a), exhibiting a comparable strength and an almost identical peak position. The distribution of the near field (insets) show how the electric fields are confined along the full chains, and particularly at the gap positions. The largest field located at one of the gaps (Figure 4a, insets) is approximately 565 and 455 times the incident field for both the straight and disordered chains, respectively. By taking the fourth power of these values, we estimate that SERS enhancements between 10 and 11 orders of magnitude may be possible.

As the introduction of disorder into the AuNR chains does not influence the resonance, further simulations were carried out on perfectly straight chains with the field polarized

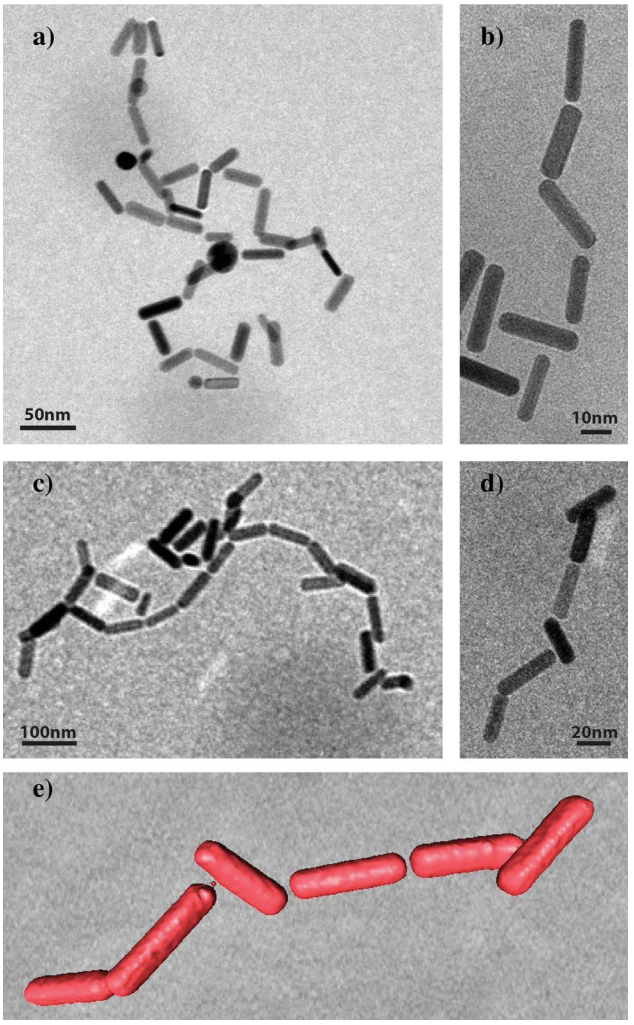

Figure 3. a–d) Cryo-TEM images of AuNRs after two washes with CB[5] showing assembly of AuNRs. e) Computer-aided visualization of the cryo-electron tomogram obtained from the assembly shown in (d), a movie can be found in the ESI.

along the axis (Figure 4b,c). The calculations emphasize the importance of narrow gaps. Figure 4b shows the resonant wavelength of the lowest energy mode for different interparticle separations and increasing number of rods per chain. All gaps considered exhibit the general behavior discussed for 1 nm gaps, with an increasing red-shift for longer chains that approaches a saturation value. Critically, narrower gaps resulted in stronger interaction between rods and thus much larger red-shifts. For example, when l_{gap} = 4 nm the lowest energy peak shifts from 725 nm for one rod to 840 nm ($\Delta\lambda$ = 115 nm) for 8 rods. In contrast, with a 1 nm gap, the corresponding shift is from 725 nm to 960 nm ($\Delta\lambda$ = 235 nm).

Figure 4c displays the enhancement corresponding to the average of the fields found at the center of each gap ($l_{gap}/2$), normalized by the strength of the illuminating plane wave. The values for the frequency of maximum enhancement are plotted, which correspond to the low energy mode. When considering a single rod, a value at a position $l_{gap}/2$ along the axis is used. With l_{gap} = 8 nm, the chaining has a relatively weak effect on the enhancement. However, for sufficiently narrow

NANO MICRO small

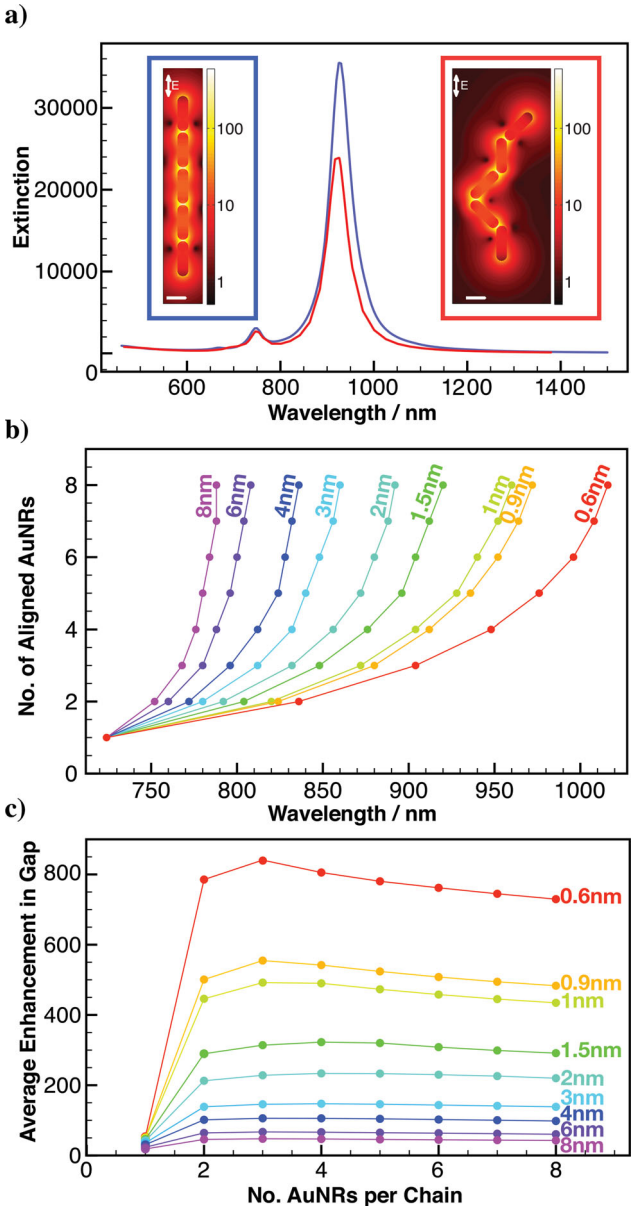

Figure 4. Calculations depicting a) the direct comparison between straight (blue) and "kinked" (red) chains of 36 nm × 11 nm AuNRs at 1 nm separation and field distribution at the lowest energy resonance for each case (insets), b) the effect of increasing chain length, on the extinction spectrum peak for straight chains, with rod separations of 0.6–8 nm and c) the effect of increasing chain length, on the average near field at the center of the gaps, for straight chains with rod separations of 0.6–8 nm.

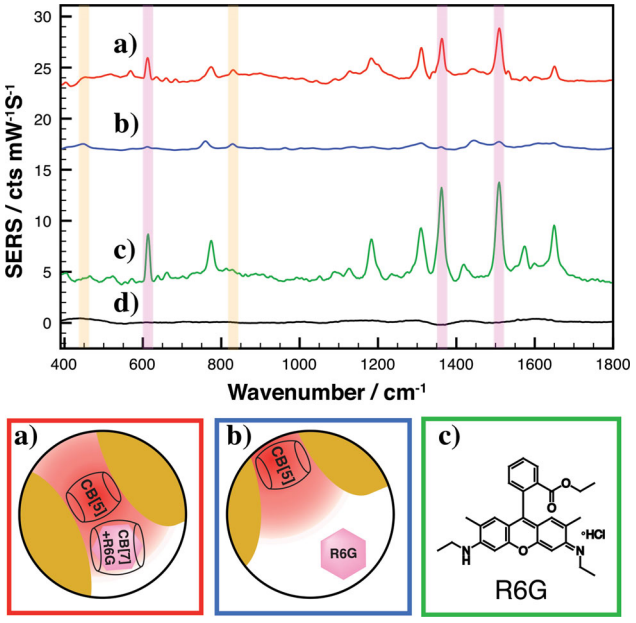

Figure 5. a) SERS spectrum and schematic representation of AuNRs washed against CB[5] and CB[7] in the presence of 100 nM R6G, b) SERS spectrum and schematic representation of AuNRs washed against only CB[5] in the presence of 100 nM R6G, c) Raman spectrum and chemical structure of R6G with characteristic peaks highlighted pink and d) SERS spectrum of AuNRs subjected to the centrifuge wash cycle in the absence of CB[*n*]. Characteristic peaks for CB[*n*] are highlighted orange.

gaps (as in CB aligned AuNRs), the field enhancement becomes significantly larger when going from single rods to the dimer, remaining relatively stable for all longer chains. Interestingly, the maximum enhancement is not necessarily found for the longest chains.[30] The achieved enhancement depends very strongly on the gap and is roughly proportional to the inverse of the gap distance.[42] Thus, long chains are not helpful to increase the field enhancement when compared to the dimer. As a consequence, for the largest gaps, the red-shift and enhancement obtained were moderate. In contrast, the combination of narrow gaps and long chains obtained in this work using CBs allows us to simultaneously obtain very significant red-shifts and large field enhancements at the inter-rod gap.

The characteristic SERS spectra of the CB macrocycle has previously been used to identify CBs between spherical NPs.[19,28] Here SERS spectra were recorded by irradiating the sample with a Raman pump laser (wavelength λ_R = 785 nm) using CB[5] to aggregate the AuNRs. These measurements show the characteristic signature for the CB wagging and stretching at 450 cm^{-1} and 825 cm^{-1}, respectively (**Figure 5**, highlighted green), confirming the presence of CB[5] between the AuNRs. A larger homologue, CB[7], has a cavity that is able to incorporate many small molecules such as methyl viologen,[43] adamantylamine,[44] amino acids such as phenylanaline,[45] and dyes such as Rhodamine 6G (R6G)[46] with high binding affinities.[47] A mixture of CB[5], CB[7] and a suitable guest resulted in the best SERS enhancements, as the CB[5] aggregates the AuNRs whilst the CB[7] binds the analyte and brings it into the SERS hot-spot. We note that this approach does not disrupt alignment of the AuNRs, and that CB[7] can also be used to align AuNRs alone (see ESI), although the formed structures and enhancements observed are then not optimal. R6G was selected to highlight the effectiveness of the CB[5]/CB[7] system as a SERS sensor as its binding within the CB[7] cavity is well known.[46] Note that the dye is pumped non-resonantly by the Raman pump so there is no electronic contribution to the SERS. Additionally, R6G has characteristic SERS absorbances at 610 cm^{-1}, 1360 cm^{-1}, 1500 cm^{-1}, and 1650 cm^{-1}, which are significantly different to the characteristic CB[*n*] absorbances (Figure 5c). When R6G was analyzed in the presence of AuNRs but

without any CB present, no SERS spectrum was observed as there were no hot-spots present (Figure 5d). Assembly of AuNRs in the presence of R6G (100 nM) and CB[5] alone, yielded only the characteristic SERS spectrum of CB[5] and trace amounts of R6G, barely distinguishable from the baseline (Figure 5b) due to the inability of R6G to occupy the hot-spot between aligned AuNRs. By contrast, the detection and enhancement of R6G (100 nM) is pronounced when CB[5] and CB[7] are used together, due to the sequestration of R6G in the hot-spot through CB[7] capture from solution (Figure 5a). An additional advantage of our nano-assembly is the specific orientation of the R6G molecules within the CB[7] to the longitudinal optical field inside the gap, selecting only certain lines from the Raman selection rules.

In conclusion, it has been shown that solution synthesized AuNRs can be successfully aligned with inter-rod separations of 0.9 nm using the macrocycle CB[*n*]. The presence of CB[*n*] at the inter-rod junction was confirmed by SERS and by analysis of TEM images giving average separations consistent with the height of one CB[*n*]. The electromagnetic simulations showed that narrow gaps are critical to obtain large field enhancement at the gaps, and that both the gap distance and the length of the assembled chain controls the red-shift, allowing for the generation of a dipolar peak well into the infrared. In addition, by combining the controlled aggregation of AuNRs at small inter-rod separations, with the larger CB homologue (CB[7]) the system has been shown to be an effective SERS based sensor for molecules in solution at very low concentrations (<100 nM). By controlling the aggregation of AuNRs with small inter-rod separations it is possible to significantly shift the absorbance into the biologically relevant region of the electromagnetic spectrum. Combining such aggregates with the host-guest ability of CB[*n*] may allow for the SERS based sensing of analytes in biological relevant environments.

Supporting Information

Supporting information for this article is available on the Wiley Online Library or from the author.

Acknowledgements

The authors would like to acknowledge H. Friedrich and M. R. P. Spapens for the reconstruction and analysis of the cryo-electron tomograms and to the EPSRC for funding (EP/K028510/1, EP/G060649/1, EP/H007024/1, EP/L027151/1), to the ERC for a Starting Investigator Grant (ASPiRe, 240629) and an Advanced Grant (LINASS, 320503) and to the RS (IE120879).

[1] L. Novotny, B. Hecht, *Principles of Nano-Optics*, Cambridge University Press, Cambridge **2006**.
[2] S. A. Maier, H. A. Atwater, *J. Appl. Phys.* **2005**, *98*, 011101.
[3] U. Kreibig, M. Vollmer, *Optical Properties of Metal Clusters*, Springer, New York **1995**.
[4] V. Myroshnychenko, J. Rodriguez-Fernandez, I. Pastoriza-Santos, A. M. Funston, C. Novo, P. Mulvaney, L. M. Liz-Marzan, F. J. Garcia de Abajo, *Chem. Soc. Rev.* **2008**, *37*, 1792–1805.
[5] S. Underwood, P. Mulvaney, *Langmuir* **1994**, *10*, 3427–3430.
[6] D. K. Yi, I.-C. Sun, J. H. Ryu, H. Koo, C. W. Park, I.-C. Youn, K. Choi, I. C. Kwon, K. Kim, C.-H. Ahn, *Bioconjugate Chem.* **2010**, *21*, 2173–2177.
[7] C. Yu, J. Irudayaraj, *Anal. Chem.* **2007**, *79*, 572–579.
[8] X. Wang, Y. Li, H. Wang, Q. Fu, J. Peng, Y. Wang, J. Du, Y. Zhou, L. Zhan, *Biosens. Bioelectron.* **2010**, *26*, 404–410.
[9] G. J. Nusz, A. C. Curry, S. M. Marinakos, A. Wax, A. Chilkoti, *ACS Nano* **2009**, *3*, 795–806.
[10] X. Huang, I. H. El-Sayed, W. Qian, M. A. El-Sayed, *J. Am. Chem. Soc.* **2006**, *128*, 2115–2120.
[11] A. Lukach, K. Liu, H. Therien-Aubin, E. Kumacheva, *J. Am. Chem. Soc.* **2012**, *134*, 18853–18859.
[12] P. Pramod, K. G. Thomas, *Adv. Mater.* **2008**, *20*, 4300–4305.
[13] J. Aizpurua, G. W. Bryant, L. J. Richter, F. J. Garcia de Abajo, B. K. Kelley, T. Mallouk, *Phys. Rev. B* **2005**, *71*, 235420.
[14] H. Xu, J. Aizpurua, M. Käll, P. Apell, *Phys. Rev. E* **2000**, *62*, 4318-4324.
[15] I. Romero, J. Aizpurua, G. W. Bryant, F. J. G. D. Abajo, *Opt. Express* **2006**, *14*, 9988–9999.
[16] E. Prodan, C. Radloff, N. J. Halas, P. Nordlander, *Science* **2003**, *302*, 419–422.
[17] R. Esteban, A. G. Borisov, P. Nordlander, J. Aizpurua, *Nat. Commun.* **2012**, *3*, 825.
[18] K. K. Caswell, J. N. Wilson, U. H. F. Bunz, C. J. Murphy, *J. Am. Chem. Soc.* **2003**, *125*, 13914–13915.
[19] L. Wang, Y. Zhu, L. Xu, W. Chen, H. Kuang, L. Liu, A. Agarwal, C. Xu, N. Kotov, *Angew. Chem. Int. Ed.* **2010**, *49*, 5472–5475.
[20] Y. Wang, A. E. DePrince, S. K. Gray, X.-M. Lin, M. Pelton, *J. Phys. Chem. Lett.* **2010**, *1*, 2692–2698.
[21] D. Fava, Z. Nie, M. A. Winnik, E. Kumacheva, *Adv. Mater.* **2008**, *20*, 4318–4322.
[22] K. Liu, Z. Nie, N. Zhao, W. Li, M. Rubinstein, E. Kumacheva, *Science* **2010**, *329*, 197–200.
[23] K. Liu, A. Lukach, K. Sugikawa, S. Chung, J. Vickery, H. Therien- Aubin, B. Yang, M. Rubinstein, E. Kumacheva, *Angew. Chem. Int. Ed.* **2014**, *53*, 2648–2653.
[24] K. D. Osberg, M. Rycenga, N. Harris, A. L. Schmucker, M. R. Langille, G. C. Schatz, C. A. Mirkin, *Nano Lett.* **2012**, *12*, 3828–3832.
[25] A. Lee, G. F. S. Andrade, A. Ahmed, M. L. Souza, N. Coombs, E. Tumarkin, K. Liu, R. Gordon, A. G. Brolo, E. Kumacheva, *J. Am. Chem. Soc.* **2011**, *133*, 7563–7570.
[26] K. Liu, A. Ahmed, S. Chung, K. Sugikawa, G. Wu, Z. Nie, R. Gordon, E. Kumacheva, *ACS Nano* **2013**, *7*, 5901–5910.
[27] T.-C. Lee, O. A. Scherman, *Chem. Eur. J.* **2012**, *18*, 1628–1633.
[28] R. W. Taylor, T.-C. Lee, O. A. Scherman, R. Esteban, J. Aizpurua, F. M. Huang, J. J. Baumberg, S. Mahajan, *ACS Nano* **2011**, *5*, 3878–3887.
[29] S. Kasera, F. Biedermann, J. J. Baumberg, O. A. Scherman, S. Mahajan, *Nano Lett.* **2012**.
[30] R. W. Taylor, R. Esteban, S. Mahajan, R. Coulston, O. A. Scherman, J. Aizpurua, J. J. Baumberg, *J. Phys. Chem. C* **2012**, *116*, 25044–25051.
[31] J. Gao, C. M. Bender, C. J. Murphy, *Langmuir* **2003**, *19*, 9065–9070.
[32] Z. Nie, D. Fava, E. Kumacheva, S. Zou, G. C. Walker, M. Rubinstein, *Nat. Mater.* **2007**, *6*, 609–614.
[33] C. Kinnear, H. Dietsch, M. J. D. Clift, C. Endes, B. Rothen- Rutishauser, A. Petri-Fink, *Angew. Chem. Int. Ed.* **2013**, *52*, 1934–1938.

[34] W. Shi, J. Casas, M. Venkataramasubramani, L. Tang, *ISRN Nanomater.* **2012**.
[35] J. Lagona, P. Mukhopadhyay, S. Chakrabarti, L. Isaacs, *Angew. Chem. Int. Ed.* **2005**, *44*, 4844–4870.
[36] H. Friedrich, P. M. Frederik, G. deWith, N. A. J. M. Sommerdijk, *Angew. Chem. Int. Ed.* **2010**, *49*, 7850–7858.
[37] F. J. Garcia de Abajo, A. Howie, *Phys. Rev. B* **2002**, *65*, 115418.
[38] T. Sannomiya, J. Vörös, C. Hafner, *J. Comput. Theor. Nanosci.* **2009**, *6*, 749–756.
[39] NIST Disclaimer: The full description of the procedures used in this paper requires the identification of certain commercial products and their suppliers. The inclusion of such information should in no way be construed as indicating that such products or suppliers are endorsed by NIST or are recommended by NIST or that they are necessarily the best materials, instruments, software or suppliers for the purposes described.
[40] P. B. Johnson, R. W. Christy, *Phys. Rev. B* **1972**, *6*, 4370–4379.
[41] R. Esteban, R. W. Taylor, J. J. Baumberg, J. Aizpurua, *Langmuir* **2012**, *28*, 8881–8890.
[42] H. Xu, E. J. Bjerneld, J. Aizpurua, P. Apell, L. Gunnarsson, S. Petronis, B. Kasemo, C. Larsson, F. Hook, M. Kall, *Proc. SPIE* **2001**, *4258*, 35–42.
[43] H.-J. Kim, W. S. Jeon, Y. H. Ko, K. Kim, *Proc. Natl. Acad. Sci.* **2002**, *99*, 5007–5011.
[44] S. Moghaddam, C. Yang, M. Rekharsky, Y. H. Ko, K. Kim, Y. Inoue, M. K. Gilson, *J. Am. Chem. Soc.* **2011**, *133*, 3570–3581.
[45] J. M. Chinai, A. B. Taylor, L. M. Ryno, N. D. Hargreaves, C. A. Morris, P. J. Hart, A. R. Urbach, *J. Am. Chem. Soc.* **2011**, *133*, 8810–8813.
[46] T. A. Martyn, J. L. Moore, R. L. Halterman,W. T. Yip , *J. Am. Chem. Soc.* **2007**, *129*, 10338–10339.
[47] M. V. Rekharsky, T. Mori, C. Yang, Y. H. Ko, N. Selvapalam, H. Kim, D. Sobransingh, A. E. Kaifer, S. Liu, L. Isaacs, W. Chen, S. Moghaddam, M. K. Gilson, K. Kim, Y. Inoue, *Proc. Natl. Acad. Sci.* **2007**, *104*, 20737–20742.

Received: April 17, 2014
Published online: July 28, 2014

